



Current status of emerging hypoxia in a eutrophic estuary: The lower reach of the Pearl River Estuary, China



Wei Qian^{a,b}, Jianping Gan^c, Jinwen Liu^a, Biyan He^d, Zhongming Lu^c, Xianghui Guo^a, Deli Wang^a, Ligu Guo^a, Tao Huang^a, Minhan Dai^{a,*}

^a State Key Laboratory of Marine Environmental Science, Xiamen University, Xiamen 361100, China

^b College of Geographical Sciences and Institute of Geography, Fujian Normal University, Fuzhou 350007, China

^c Department of Mathematics and Division of Environment, Hong Kong University of Science and Technology, Kowloon, Hong Kong, China

^d College of Food and Biological Engineering, Jimei University, Xiamen 361021, China

ARTICLE INFO

Article history:

Received 17 September 2017

Received in revised form

30 January 2018

Accepted 4 March 2018

Available online 8 March 2018

Keywords:

Pearl River (Zhujiang River) Estuary

Dissolved oxygen

Hypoxia

Eutrophication

ABSTRACT

We examine the current status of dissolved oxygen (DO) and its trend over the past 25 years in the lower Pearl River Estuary, a large eutrophic estuary located in Southern China and surrounded by large cities including Hong Kong, Shenzhen and Guangzhou. Monthly cruises conducted from April 2010 to March 2011 clearly show that DO depletion began to emerge in the bottom layer of the lower estuary off Hong Kong in June, and became fully developed in July and August when oxygen-deficient water occupied ~1000 km² before gradually becoming re-oxygenated in September and October. The development of the low oxygen zone was closely coupled with phytoplankton blooms in the surface water, which was supersaturated with respect to DO suggesting the importance of autochthonous organic matter in fueling bottom DO consumption after settling through the pycnocline. Long-term monitoring data collected in the study area adjacent to Hong Kong by the Hong Kong Environmental Protection Department showed a decreasing trend of $-2 \pm 0.9 \mu\text{mol kg}^{-1} \text{yr}^{-1}$ in the annual minimum DO concentration in bottom water over the past 25 years. Associated with the decrease in DO was an increase in the annual maximum surface concentration of dissolved inorganic nitrogen (DIN) at a rate of $\sim 1.4 \pm 0.3 \mu\text{mol kg}^{-1} \text{yr}^{-1}$, suggesting again that eutrophication is the most plausible driver of oxygen deficiency in this region. Therefore, our monthly cruises, along with the decadal monitoring data, reveal a large low oxygen zone, likely developing into a large hypoxic zone driven primarily by anthropogenic eutrophication. This new development suggests environmental stressors such as eutrophication may have a cascading effect, with important and expensive consequences for the regional environment.

© 2018 Elsevier Ltd. All rights reserved.

1. Introduction

Hypoxia is an important symptom of coastal environment degradation (Chen et al., 2007; Shen et al., 2008; Alvise and Cozzi, 2016; Zhu et al., 2016; Zhao et al., 2017). It has led to mass mortality of impacted marine organisms and changes in seawater chemistry, altering elemental biogeochemistry and enhancing coastal acidification (Kristiansen et al., 2002; Rabalais et al., 2002; Grantham et al., 2004; Cai et al., 2011). The area of the coast which suffers from hypoxia has rapidly expanded and now covers more

than 245,000 km² globally (Diaz and Rosenberg, 2008). Coastal hypoxia has increasingly become a worldwide issue of concern for both the scientific community and the general public (Dai et al., 2006; Diaz and Rosenberg, 2008; Bianchi and Allison, 2009; Friedrich et al., 2014; Wang et al., 2016; Su et al., 2017).

The Pearl River, the second largest river in China in terms of freshwater discharge, has experienced large biogeochemical alterations due to rapid urbanization and industrialization within its watershed and delta over the past three decades (Jia and Peng, 2003; Wang et al., 2012, 2015; Dai et al., 2014; Wu et al., 2016). In previous studies, year-round hypoxia throughout the water column has been observed in the upper Pearl River Estuary (PRE), where extremely high $p\text{CO}_2$ ($>4000 \mu\text{atm}$), concentrations of organic matter ($\sim 400 \mu\text{mol C L}^{-1}$ for DOC, $\sim 200 \mu\text{mol C L}^{-1}$ for POC), dissolved inorganic nitrogen (DIN $150\text{--}1000 \mu\text{mol L}^{-1}$), and N_2O

* Corresponding author. State Key Lab of Marine Environmental Science, Xiamen University, Xiamen 361005, China.

E-mail address: mdai@xmu.edu.cn (M. Dai).

production suggest the presence of enhanced biogeochemical processes such as aerobic respiration and nitrification (Zhai et al., 2005; Dai et al., 2006; He et al., 2014; Lin et al., 2016). In the lower PRE, only episodic hypoxic events have been reported despite its highly eutrophic nature primarily based on the surveys in the 1990's and 2000's (Harrison et al., 2008; Rabouille et al., 2008; Xu et al., 2010). This episodic hypoxia, which contrasts to the lower regions of other large estuaries such as the Changjiang and Mississippi which experience sustained hypoxia seasonally, has been interpreted to be related to the dynamic physical settings of the lower PRE and its shallow depth, the latter which results in short water residence times (~3–5 day) during periods of high discharge in the summer (Yin et al., 2004a; Ye et al., 2013; Zu and Gan, 2015). However, it remains unknown whether this environment will avoid the onset of sustained hypoxia under more severe eutrophic conditions since these prior researches. It is therefore crucial to reexamine the current status of DO in the lower PRE under sustained eutrophic conditions.

Here we present our field observations during monthly surveys from April 2010 to March 2011 in the PRE. Additionally, we integrate long-term monitoring data at selected stations in the lower PRE off Hong Kong. We aim to assess the current status of DO in the estuary and its long-term evolution over the past few decades. Here we define hypoxia as a dissolved oxygen (DO) concentration of $<2 \text{ mg L}^{-1}$ following SCOR working group #128 (Levin et al., 2009; Middelburg and Levin, 2009; Zhang et al., 2010). We also defined oxygen deficiency as $\text{DO} < 3 \text{ mg L}^{-1}$, or $< 90 \mu\text{mol kg}^{-1}$, which is a slightly stricter standard than quantitative conversion of mg L^{-1} values (3 mg L^{-1} is equivalent to $92 \mu\text{mol kg}^{-1}$ when $S = 30$ and temperature = 20°C).

2. Materials and methods

2.1. Study area

The Pearl River extends more than 2200 km, and has a drainage area of $4.5 \times 10^5 \text{ km}^2$ containing 6 provinces of southern China as well as Hong Kong and Macau (Dai et al., 2014 and references therein). The Pearl River flows into the northern South China Sea via eight outlets through three sub-estuaries. The Lingdingyang bay (also called the PRE in this work) is the largest sub-estuary of the Pearl River with a surface area of $\sim 2000 \text{ km}^2$, receiving 53% of the total river discharge from four eastern outlets (Humen, Jiaomen, Hongqimen, Hengmen). The PRE as a whole is funnel-shaped, starting at $\sim 4 \text{ km}$ wide at the northern end near the Humen outlet and gradually widening to $\sim 26 \text{ km}$ between Macau and Lantau Island (Fig. 1). Seaward of the PRE, the direction of the river plume is largely driven by the seasonally reversing East Asian monsoon and coastal currents, generally turning east in the presence of intensified upwelling during the summer, and west during the winter (Qu et al., 2004; Su, 2004; Gan et al., 2009; Cao et al., 2011; Han et al., 2012; Dai et al., 2014). This estuary has undergone intensive anthropogenic perturbations, such as domestic sewage, industry wastewater discharge, fertilizer usage and runoff, resulting in a number of environmental issues (Dai et al., 2008; Lu et al., 2009; He et al., 2014). For example, the annual consumption of agricultural fertilizer and total wastewater discharge in Guangdong Province gradually increased from 1.10 (1985) to 2.56 (2015) million tons (<http://data.stats.gov.cn/easyquery.htm>) and from ~ 2.5 (1990) to ~ 9.0 (2015) billion tons (<http://www.gdep.gov.cn>), respectively.

2.2. Cruises, sampling and data sources

Twelve cruises were conducted monthly from April 2010 to

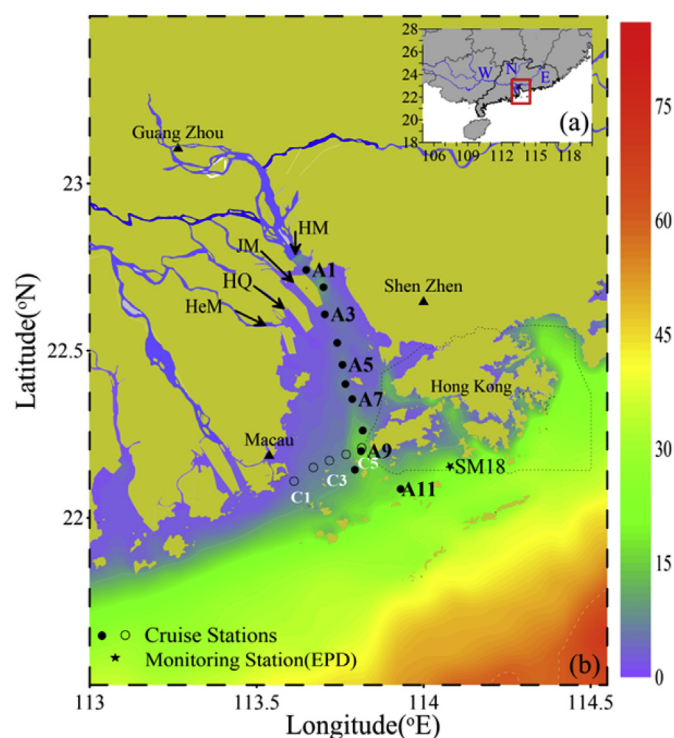


Fig. 1. (a) Map of the whole Pearl River showing the three main tributaries, namely the West River (W), North River (N) and East River (E). The red rectangle denotes our study site. (b) Map of sampling stations showing the stations of latitudinal Transect A (●) and longitudinal Transect C (○) during our 2010–2011 cruises. The long-term monitoring station SM18, operated by the Hong Kong EPD, is denoted by an asterisk. Four outlets of the Pearl River (HM for Hu Men, JM for Jiao Men, HQ for Hongqi Men and HeM for Heng Men) are marked by arrows. (For interpretation of the references to colour in this figure legend, the reader is referred to the Web version of this article.)

March 2011 along a cross-estuary transect (Transect C) between Macau and Hong Kong (Fig. 1). Additionally, an along-estuary transect (Transect A) was conducted seasonally during January, April, August and November (representing winter, spring, summer and autumn, respectively), consisting of 10–11 stations stretching from the Humen outlet to coastal waters off Hong Kong. In order to capture the temporal variability of the system, the 12 cruises were categorized into four seasons: December to February the following year for winter, March to May for spring, June and August for summer, and September to November for autumn. Here we refer to the summer months as the wet season and the remaining months as the dry season (Han et al., 2012).

In addition to cruise data, this study examines long-term monitoring results at Station SM18 dating back to February 1990. SM18 is located at $22^\circ 9.211' \text{N}$, $113^\circ 57.727' \text{E}$ in $\sim 21 \text{ m}$ of water depth, south of Hong Kong and northeastward of the estuary's mouth. This location is influenced by the river plume in the summer and by coastal marine water in the winter (Ou et al., 2009; Zu et al., 2014). The ~ 25 -year monitoring project at SM18 was operated by the Hong Kong Environmental Protection Department (HK-EPD, <http://www.epd.gov.hk/epd/>). Yin et al. (2004a) reported results from the first 10 years of the dataset (1990–2000), showing that bottom water DO dropped from the 1980's to the 1990's.

2.3. Materials and methods

During the cruises, water samples were collected with Niskin bottles equipped with CTD sensors (SBE 25 Sea logger CTD). A subset of salinity data from Transect A has previously been reported

by Lu and Gan (2015). DO values were determined onboard with $\sim 1 \mu\text{mol kg}^{-1}$ precision using the Winkler titration method, as described previously (Dai et al., 2006; Guo et al., 2009). Nutrient samples were filtered through $0.45 \mu\text{m}$ cellulose acetate fiber membranes, with the first $\sim 100 \text{ mL}$ of filtrate discarded and $\sim 50 \text{ mL}$ collected for $\text{NO}_3\text{-N}$ and $\text{NO}_2\text{-N}$ measurements. Nutrient samples were stored at -20°C in pre-cleaned HDPE bottles until analysis in the land-based laboratory at Xiamen University. $\text{NO}_3\text{-N}$ and $\text{NO}_2\text{-N}$ were analyzed by reducing $\text{NO}_3\text{-N}$ to $\text{NO}_2\text{-N}$ through a copper-cadmium column and subsequently measuring $\text{NO}_2\text{-N}$ with a pink azo dye method on a Technicon AA3 Auto-Analyzer (Bran-Lube, GmbH), as previously described (Dai et al., 2008; Han et al., 2012). $\text{NH}_4\text{-N}$ was determined based on the standard indophenol blue method onboard the ship (Yan et al., 2012). *Chl a* samples were filtered onto 25 mm glass fiber membranes ($0.7 \mu\text{m}$ nominal pore size) under pressures $< 100 \text{ mmHg}$, and then kept at -20°C prior to analysis. In the laboratory, the membranes were extracted with 90% acetone before determination of *Chl a* concentrations with a fluorimeter (Parsons et al., 1984; Herbland et al., 1985). The analytical precision was 1% and 10% for $\text{NO}_3\text{-N}$ and $\text{NO}_2\text{-N}$ and *Chl a*, respectively.

The long-term monitoring dataset from 1990 to 2014 at Station SM18 was acquired from the website of the Hong Kong EPD (http://www.epd.gov.hk/epd/english/environmentinhk/water/marine_quality/mwq_report.html) and included temperature, salinity, DIN ($\text{NO}_3\text{-N} + \text{NO}_2\text{-N} + \text{NH}_4\text{-N}$), DO and *Chl a* data. The analytical protocols for temperature, salinity, DO, *Chl a* and DIN were consistent throughout the duration of the monitoring campaign (<http://wqrc.epd.gov.hk/en/water-quality/marine-2.aspx>). The high degree of similarity of data collected by the Hong Kong EPD and during our monthly cruises in 2010 and 2011 underscores the quality of the monitoring data. Additionally, the observed decline in DO over the period of the long-term monitoring dataset is consistent with historical and recent surveys (Yin et al., 2004a; Ye et al., 2012, 2013; Su et al., 2017). This valuable dataset has been used in several publications over the last ten years (Yin et al., 2004a; Xu et al., 2008, 2010, 2011; Lui and Chen, 2011, 2012).

3. Results

3.1. Hydrological characteristics of the PRE during the 2010 and 2011 cruises

During the winter, surface water temperatures were generally $< 20^\circ\text{C}$ throughout Transect A (Fig. S1). Relatively warmer water of $\sim 20^\circ\text{C}$ was found downstream along the cross-estuary Transect C in December, although temperatures dropped to $\sim 15^\circ\text{C}$ by February before gradually increasing to $\sim 24^\circ\text{C}$ in May. In the summer, the warmest water was found predominantly in the upper estuary. Meanwhile, in the lower estuary, cooler water of $\sim 24^\circ\text{C}$ intruded from offshore beneath the warm surface freshwater layer, creating a distinct thermocline. In autumn, the surface water cooled to $\sim 22^\circ\text{C}$ and the vertical temperature difference in the water column gradually diminished.

The salinity distributions were consistent with changes in temperature. The water column was largely vertically homogeneous during the winter and spring until May, when stratification began to form. In the summer, low salinity water ($S < 10$) dominated the upper estuary, and mid-estuary water ($S < 20$) gradually inundated the surface layer over the estuary starting in June, which lasted throughout the summer. At the same time, higher salinity coastal water (salinity = ~ 34 at the bottom of A11, the southernmost station, Fig. S2) formed a clear salt wedge at the lower reach of the estuary during July and August. Therefore, the vertically homogeneous salinity profile near the Humen outlet transitioned into a

stratified water column in the lower reach of the estuary, especially in the vicinity of the estuarine mouth where the vertically homogeneous salinity profile was re-established in mid-autumn and persisted until the following late spring.

The seasonal variations of density were highly similar to those of salinity (see in Fig. 2). There was a prominent horizontal density gradient from ~ 1000 to $\sim 1020 \text{ kg m}^{-3}$ throughout the year along Transect A. The intense vertical stratification began in May, peaked in the summer when lighter freshwater inundated the saline bottom water and created a distinct surface layer, and gradually faded by autumn at Transect C.

3.2. Spatial and temporal variations of nutrients, DO and *Chl a*

DIN concentrations displayed a remarkable decline from the Humen outlet to the entrance of the PRE (Fig. S3). The DIN concentrations in the fresh and brackish water near the Humen outlet were extremely high ($\text{DIN} > 100 \mu\text{mol kg}^{-1}$) throughout the year. Nutrient-rich water was distributed unevenly with a tendency towards decreasing concentrations from west to east along Transect C, resulting in $\sim 20 \mu\text{mol kg}^{-1}$ DIN at the easternmost station (C5) in winter. From April to August, the vertical distribution of DIN transitioned from well mixed to stratified in the lower estuary. The high DIN water ($> 50 \mu\text{mol kg}^{-1}$) was observed extending to the surface layer of Transect C and its vicinity during the August cruise. In autumn, Transect C was dominated by DIN depleted water and the nutrient-rich water was mainly constrained to the westernmost station near the coast.

Remarkable spatiotemporal variations in DO occurred in the PRE (Fig. 3). A low DO center ($\text{DO} = 109 \pm 39 \mu\text{mol kg}^{-1}$, $n = 9$, or $43 \pm 15\%$ saturated during the spring, summer and autumn; $\text{DO} = 189 \pm 11 \mu\text{mol kg}^{-1}$, $n = 3$, or $\sim 68 \pm 9\%$ saturated during the winter) containing low salinity water was clearly observed near the Humen outlet throughout all four seasons during our surveys. Low DO water in this region is believed to originate from upstream (He et al., 2014 and references herein). In contrast, DO displayed significant seasonality downstream of the Humen outlet. In the winter, DO values were $> 200 \mu\text{mol kg}^{-1}$ ($> 85\%$ saturated) in the lower estuary throughout Transect C. In the spring, surface water DO values increased to $> 300 \mu\text{mol kg}^{-1}$ and the DO saturation state reached $> 120\%$ by May, and DO-deficient bottom water had not yet appeared. In the summer, DO-deficient water gradually occupied the bottom layer of Transect C and the southernmost stations of Transect A where DO dropped to $< 20 \mu\text{mol kg}^{-1}$ in July. DO concentrations were $\sim 60 \mu\text{mol kg}^{-1}$ in bottom layer by August when the surface water DO was greatly oversaturated ($> 130\%$) downstream of Station A7. DO then gradually recovered to $> 170 \mu\text{mol kg}^{-1}$ ($> 80\%$ saturated) throughout the water column by mid-autumn in October. We also observed that the vertical structure of DO resembled the distribution of salinity, suggesting the impact of the stratification on DO values. In contrast to being vertically homogeneous from October to the following April, DO distributions were strongly stratified from June to August in the lower estuary.

Surface *Chl a* concentrations were also highly variable throughout the estuary (Fig. S4). High *Chl a* concentrations ($> 5 \mu\text{g L}^{-1}$) were observed in the surface layer both near the Humen outlet (Latitude $> 22.6^\circ\text{N}$) in August and in the lower estuary from late spring (May) to early autumn (September). The high *Chl a* center upstream near the Humen outlet was frequently observed coinciding with low concentrations of DO and high $p\text{CO}_2$, indicating high rates of respiration and net heterotrophy (Zhai et al., 2005; Guo et al., 2009). Another remarkably high *Chl a* center was found near the entrance of the estuary between Hong Kong and Macau along Transect C, where oversaturated DO values indicate high

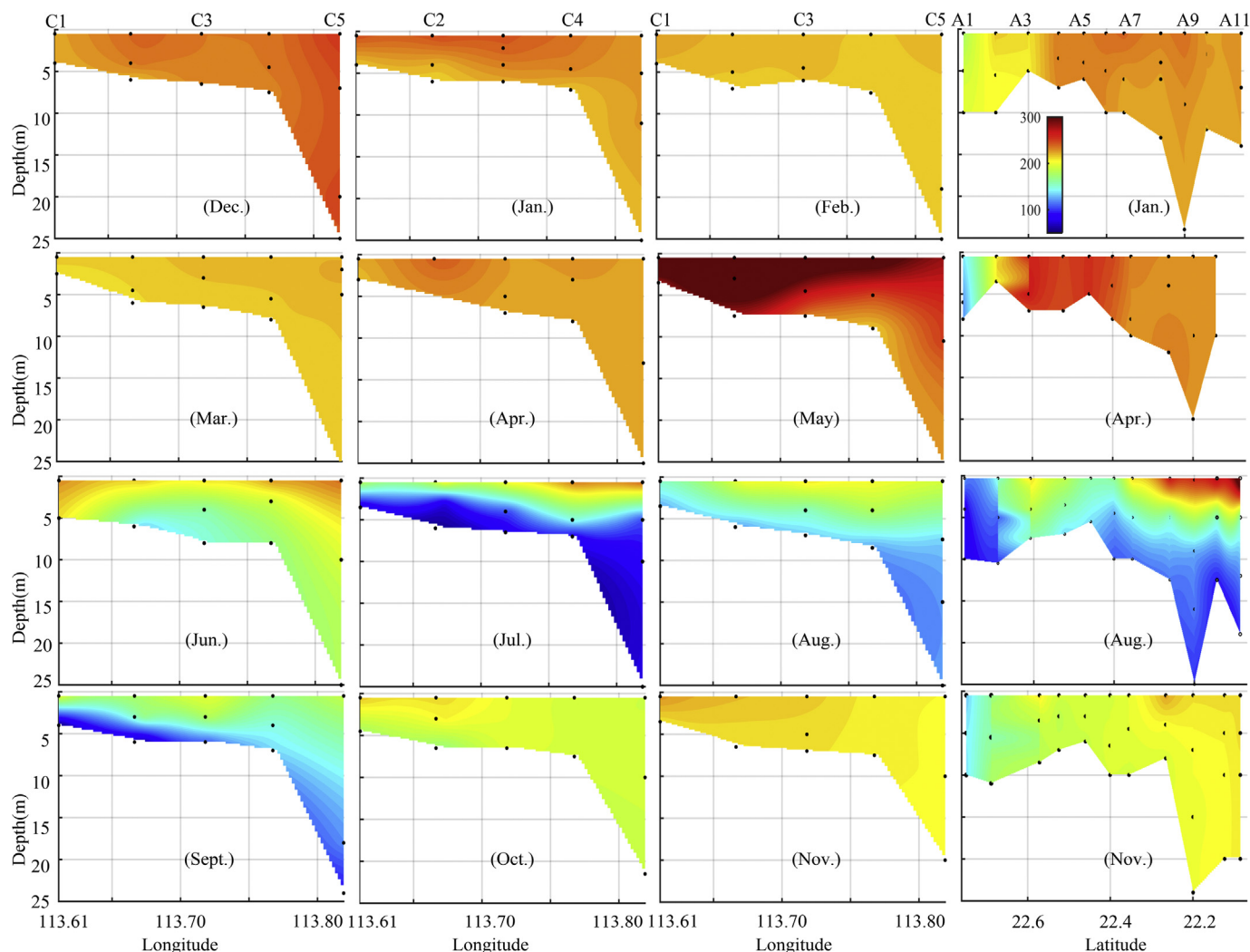


Fig. 2. Density (kg m^{-3}) distributions along Transects C and A during monthly cruises from April 2010–March 2011 in the PRE. All cruises were categorized into (a) winter, (b) spring, (c) summer and (d) autumn.

rates of primary production from algal blooms nearby (Tang et al., 2003; Guo et al., 2009; Lu and Gan, 2015).

3.3. Long-term monitoring stations off Hong Kong

The EPD long-term monitoring station (SM18) is located ~30 km eastward of Transect C and south of Hong Kong. Similar to our cruise data, surface water temperatures also showed distinct seasonal variations, rising from ~15 °C in winter to ~30 °C in summer (Fig. 4a). During most of the year, the temperature of the bottom water was nearly identical to the surface and both fluctuated with similar patterns. Relatively cooler water masses (~24 °C) often emerged in the bottom layer during mid-summer, which deviated, as expected, from surface temperatures under stratified conditions.

Significant variations in surface salinity, which ranged between 10 and 33, were observed (Fig. 4b). The annual minimum salinity consistently appeared during mid-year when freshwater discharge rates were the highest. Salinity was relatively invariable in the bottom layers throughout the survey period. Overall, the water column was well-mixed during most of the dry seasons and highly stratified during the wet seasons.

Two general types of DO patterns were observed as a function of thermohaline variations (Fig. 4c). The first featured both surface

and bottom waters that were uniformly well oxygenated (~220 $\mu\text{mol DO kg}^{-1}$), and close to the DO solubility at $S = 30$ and $T = 20$ °C. The second featured oversaturated DO (~250 $\mu\text{mol kg}^{-1}$) in the surface waters with deoxygenated or even hypoxic conditions in the bottom waters. These two patterns were generally consistent with the well-mixed conditions observed during the dry seasons versus the stratified conditions of the water column in the wet seasons.

During most of the dry seasons, relatively lower DIN concentrations were observed throughout the water column (Fig. 4d). Remarkably higher values showing large variations in DIN were observed in the surface layer during summer months, especially during 2005–2006, 2008–2009, and in 2013. These high values typically occurred when salinity was relatively low, suggesting the influence of nutrient-rich freshwater. In subsurface water, DIN concentrations were generally lower than ~20 $\mu\text{mol kg}^{-1}$. Surface *Chl a* values also displayed large variations throughout the annual cycles (Fig. 4e). During most years, *Chl a* concentrations peaked during the summer (mid-year) with values > 10 $\mu\text{g L}^{-1}$, but exhibited much lower values during the rest of the year, indicating that phytoplankton blooms predominantly occurred during summer. The monthly variations of each parameter are displayed in boxplots (Fig. 4f–o) which show their distinct seasonality. In dry

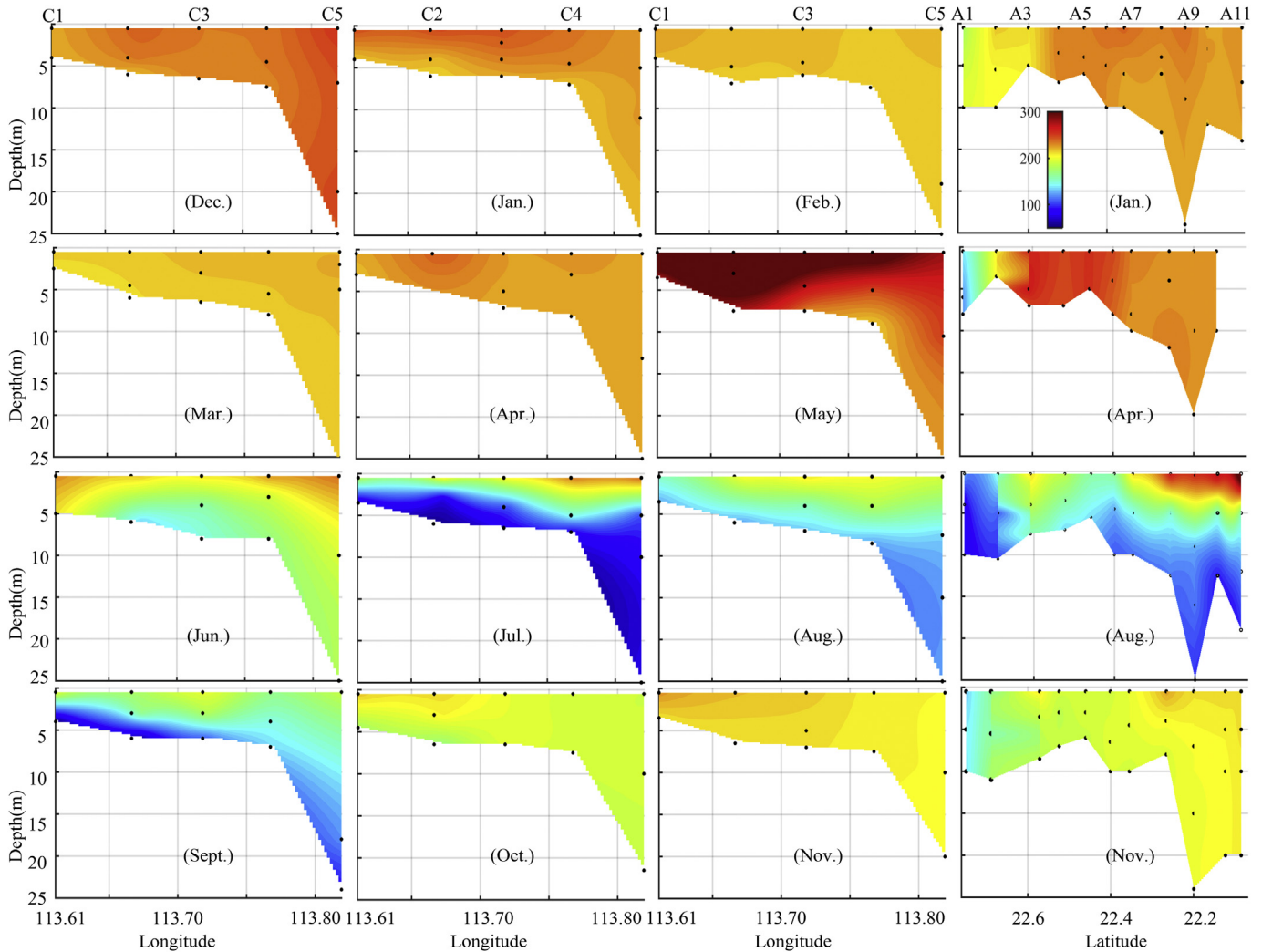


Fig. 3. DO ($\mu\text{mol kg}^{-1}$) distributions along Transects C and A during monthly cruises from April 2010–March 2011 in the PRE. Note that DO values higher than $300 \mu\text{mol kg}^{-1}$ were rendered equally to $300 \mu\text{mol kg}^{-1}$ for simplification.

seasons, the water column was generally homogeneous and well oxygenated with low concentrations of DIN and *Chl a*, but highly stratified with benthic DO-deficient water in wet seasons.

The fluctuations of most parameters measured at Station SM18 strongly resembled those at Station C5, the easternmost station of Transect C, from April 2010 to March 2011. Based on DO values at Station SM18 ($\text{DO} = \sim 30 \mu\text{mol kg}^{-1}$, $\sim 16\%$ saturated in August 2010) and our survey results in August 2010, the DO-deficient water was estimated to occupy $\sim 1000 \text{ km}^2$ from the mid-estuary extending offshore of Hong Kong (Fig. 5). It is worth noting that DO distributions nearshore off Macau and even the offshore regions are still unclear due to the limited coverage of our surveys. Recent surveys in the summer confirmed that this area is subject to DO deficient and/or hypoxic conditions (Ye et al., 2013; Su et al., 2017). Therefore, the area of DO deficient water estimated here should be regarded as a lower limit.

4. Discussion

4.1. Eutrophication and deoxygenation trends

The yearly maximum value of surface DIN ranged from ~ 13 to $\sim 100 \mu\text{mol kg}^{-1}$, coinciding with large variations in salinity (from

12.6 to 31.7), at Station SM18. In order to differentiate the impact of eutrophication versus physical mixing on these trends, the regional normalization method (Cao et al., 2011) is adopted to normalize DIN to nDIN ($S_{\text{ref}} = 21$, the average salinity value for DIN samples).

$$\text{nDIN} = \frac{\text{DIN}_m - \text{DIN}_s}{S_m - S_s} \times (S_{\text{ref}} - S_s) + \text{DIN}_s \quad (1)$$

In equation (1), nDIN is the normalized DIN value, DIN_s and S_s are defined as the sea end-member values (designated as $\text{DIN}_s = 0$ and $S_s = 35$, respectively), and DIN_m and S_m are the measured values. nDIN exhibited a significant increasing trend at a rate of $\sim 1.4 \pm 0.3 \mu\text{mol kg}^{-1} \text{ yr}^{-1}$, indicating an increase in eutrophication over the past several decades in this large estuary and coastal region (see in Fig. 6a).

Annual maximum *Chl a* values in the surface layer ranged from 1.3 to $35 \mu\text{g L}^{-1}$, and the relatively lower concentrations ($< 10 \mu\text{g L}^{-1}$) were only observed before 2000. The increasing trend was significant for annual maximum *Chl a* values (\log_{10} transformed), suggesting an incremental $\sim 4\%$ increase annually over the last 25 years (Fig. 6b).

Yin et al. (2004a) suggested there was no apparent decreasing trend in DO based on bimonthly monitoring data from 1990 to 2000. It is noteworthy that the annual minimum DO saturation of

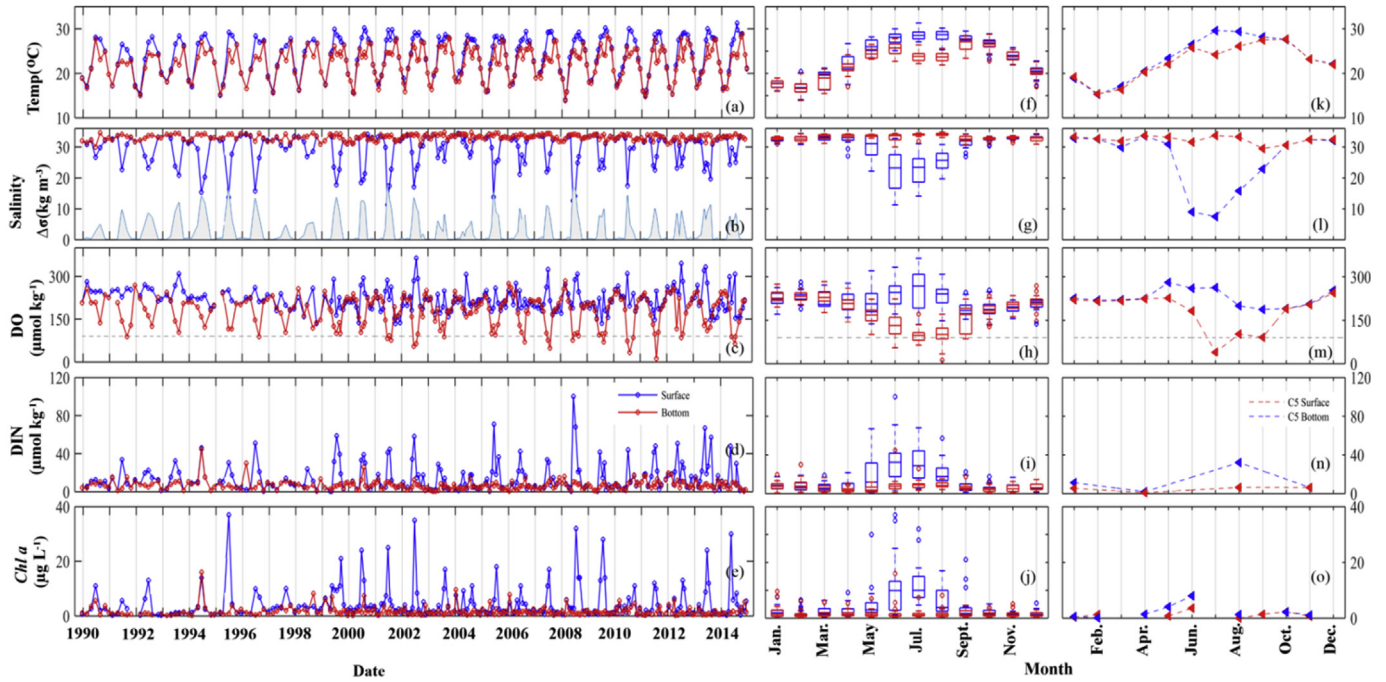


Fig. 4. Long-term variations in (a) temperature, (b) salinity (superimposed on $\Delta\sigma$, the shaded area, which is the difference between surface and bottom water density), (c) DO, (d) DIN and (e) *Chl a* at the surface (blue) and bottom (red) during February 1990 to December 2014 at SM18. The criterion of hypoxia ($90 \mu\text{mol kg}^{-1}$) is shown with dashed lines in the DO panels. Boxplots (from f to j) are shown for the corresponding parameters in each month at SM18. The edges of the open boxes indicate the 25th and 75th percentiles whereas the central mark is the median. The whiskers extend to the most extreme data points not considered individually. The closed triangles denote the corresponding samples from Station C5 from April 2010 to March 2011 (from k to o). (For interpretation of the references to colour in this figure legend, the reader is referred to the Web version of this article.)

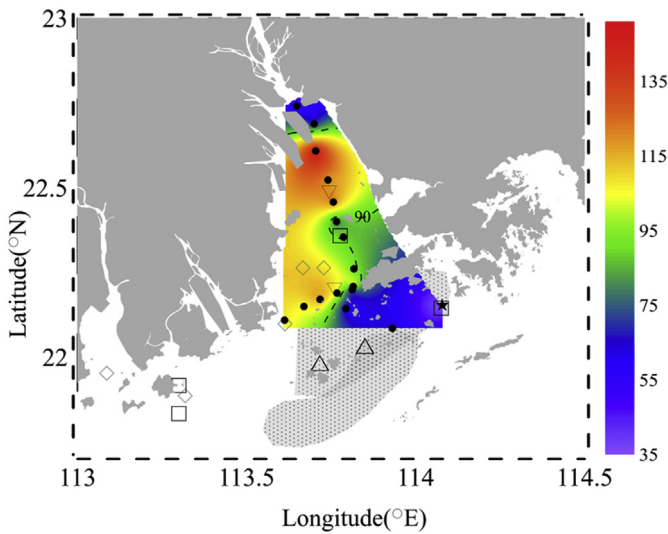


Fig. 5. The estimated DO-deficient zone ($<90 \mu\text{mol kg}^{-1}$) at the bottom of the PRE during the August 2010 cruise. Also shown are the historical summer hypoxia ($\text{DO} < 3 \text{ mg L}^{-1}$, $\sim 90 \mu\text{mol kg}^{-1}$) locations reported in the PRE and adjacent coastal waters. \square indicates stations reported in Lin et al. (2001), \diamond for Yin et al. (2004a), ∇ for Luo et al. (2005), and \triangle for Ye et al. (2013), and \bullet for monthly survey stations. Additionally, the shaded area denotes the DO-deficient zones revealed in the summer of 2014 (Su et al., 2017).

bottom water emerged during the summer months (June to August) when hypoxia was prone to occur. The decreasing trend of annual minimum bottom water DO was not significant from 1990 to 2000 ($-0.66 \pm 0.7\% \text{ yr}^{-1}$, $p = 0.39$), but was significant from 1990 to 2014 at SM18 (Fig. 6c) with a decreasing trend of $-1.2 \pm 0.4\% \text{ yr}^{-1}$

(equivalent to $\sim 2 \pm 0.9 \mu\text{mol kg}^{-1} \text{ yr}^{-1}$, $p = 0.0047$). Moreover, this decline cannot be attributed to the increase in sampling frequency (bimonthly to monthly) after 2000, as the DO decline in the bottom water is also supported by observations from each August throughout the past 25 years (regression slope = $\sim 0.9 \pm 0.4\% \text{ yr}^{-1}$, $r = 0.43$, $p < 0.05$ in the Fig. 6c). The rapid decline indicated a change in bottom water DO status beyond the natural annual cycles, resulting in a hypoxia-favorable region in the lower estuary of the Pearl River. Though the bottom water DO dropped to $< 2 \text{ mg L}^{-1}$ only 4 times from 1990 to 2014 (June of 2002, August of 2007, 2010, 2011), DO-deficient conditions ($< 90 \mu\text{mol kg}^{-1}$) were mostly recorded after 2000 (18 out of 20 records for the whole data set). In summary, our monthly surveys and the long-term monitoring data show a decrease in DO over the past decades, indicating the lower estuary of the Pearl River has become a DO deficient and/or a seasonally hypoxic zone due to the gradual exacerbation of eutrophic conditions in this coastal ecosystem.

4.2. Mechanisms for the observed coastal hypoxia

Based on the conspicuous seasonality shown by each of the measured parameters, we discuss here in a qualitative way the possible drivers of oxygen depletion, primarily physical processes and biological activities associated with seasonal river runoff, winds and coastal currents. A more quantitative analysis of the sources of organic matter that consume oxygen is performed by Su et al. (2017).

The dry seasons were characterized by a vertically homogenous water column in most of the estuary, a westward flowing river plume accompanied by low water discharge rates, and a north-easterly monsoon (Su, 2004). Intense stratification is shown as a critical factor for the formation and maintenance of hypoxia in subsurface waters. Thus, the well-mixed water column in the lower

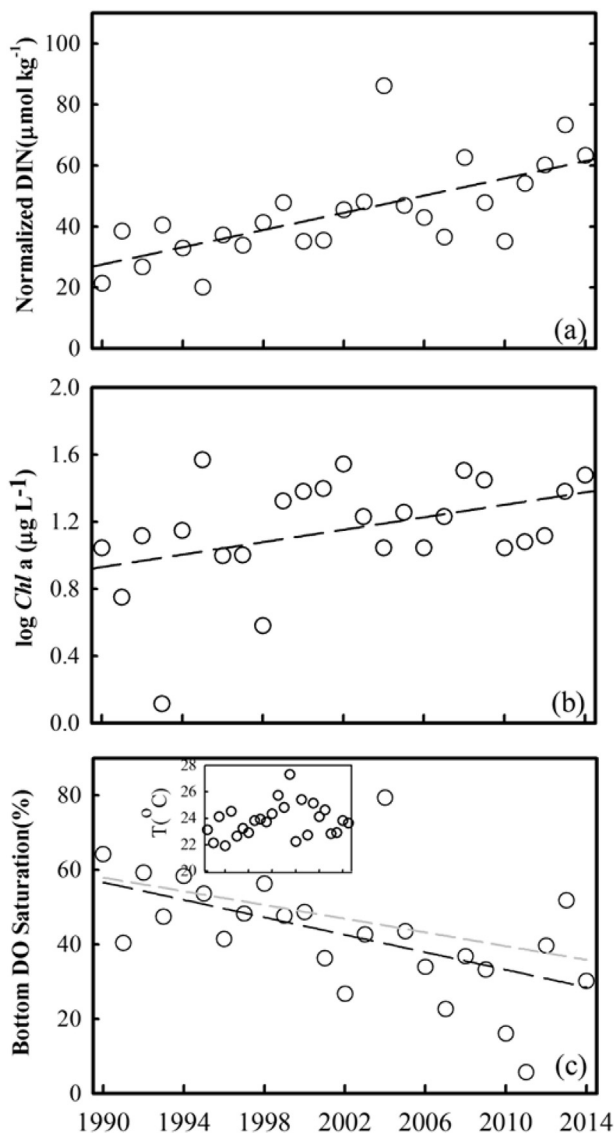


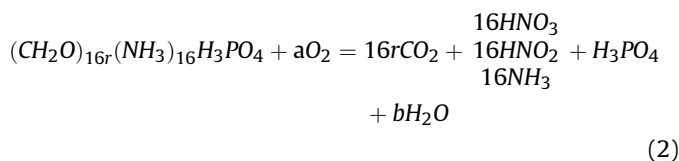
Fig. 6. (a) Normalized annual maximum DIN in the surface layer from 1990 to 2014 (all DIN data are normalized to $S = 21$, see detail in text). The dashed line denotes the linear regression of normalized DIN vs. year (slope = $1.4 \pm 0.3 \mu\text{mol kg}^{-1} \text{ year}^{-1}$, $r = 0.67$, $p < 0.01$, $n = 25$); (b) the annual maximum *Chl a* values (\log_{10} transformed) in the surface layer in the EPD data set. The dashed line denotes the linear regression (slope = 0.0186 , $r = 0.42$, $p < 0.05$, $n = 25$). (c) The trend from 1990 to 2014 of annual minimum DO saturation in the bottom layer at Station SM18. The linear regression results of bottom water DO annual minimum values are denoted (dark dashed, slope = $-1.2 \pm 0.4\% \text{ year}^{-1}$, $r = 0.55$, $p < 0.01$, $n = 25$) and the saturation state during each August (gray dashed, slope = $-0.9 \pm 0.4\% \text{ year}^{-1}$, $r = 0.41$, $p < 0.05$, $n = 25$) over the past 25 years.

estuary is likely the reason for the absence of DO-deficient water during the dry seasons even if the surface water is oversaturated with respect to DO, the latter which suggested remarkable in-situ productivity in May. Moreover, the weak stability of the water column may have inhibited phytoplankton growth when nutrient-rich brackish water was observed (Fig. S2) at C transect in January (Lu and Gan, 2015). At station SM18, DIN and *Chl a* concentrations were primarily $< 20 \mu\text{mol kg}^{-1}$ and $< 10 \mu\text{g L}^{-1}$ in dry seasons (Fig. 7a). Meanwhile, DO at near-saturation (90%–110%) together with a 1:1 linear correlation between surface and bottom water DO saturation states (Fig. 7c) clearly indicated that physical mixing overwhelmed biological activities during most of dry seasons off Hong Kong.

In wet seasons, freshwater inundated the surface layer while saline water intruded landward in the subsurface layer, forming a distinct halocline within the estuary and in nearby waters. The horizontal structure of the river plume was variable and had the highest probability of spreading offshore towards the east in July upon exiting the PRE (Ou et al., 2009; Zu and Gan, 2015). From June to September, our observations underscored the synchronicity between stratification and DO-depletion/hypoxia in the lower estuary. The seasonal low $p\text{CO}_2$ (Guo et al., 2009) and regional content of algal-derived organic carbon in the water column and sediment (Hu et al., 2006; Su et al., 2017) indicated that marine primary production was high at the outlet of Lingdingyang Bay and nearby. These physical and biological factors make the lower estuary prone to hypoxia.

At SM18 and nearby, the river plume brought in higher DIN concentrations ($> 20 \mu\text{mol kg}^{-1}$) and consequently enhanced productivity (Yin et al., 2004b; Wu et al., 2017), evidenced by high zonal *Chl a* concentrations, supersaturated DO, and lower $p\text{CO}_2$ in the surface layer (Guo et al., 2009; Cao et al., 2011; Lu and Gan, 2015). Changes in the magnitude of oversaturation of DO at the surface and the occurrence of hypoxia in bottom waters were largely synchronized, resulting in a deviation from the 1:1 ratio (Fig. 7d). This suggests that increases in DO-oversaturation in the surface waters are linked to increases in DO-deficits in the bottom layer. This result implies a close linkage between the high in-situ productivity at the surface and deoxygenation below the pycnocline. This also suggests that stratification is essential in the formation of hypoxia in the lower estuary. Our data support this, showing blooms in a mixed water column without the development of hypoxia in the spring when stratification was weak. In the summer, when the water column became stratified, surface blooms resulted in bottom water oxygen-deficiency in the lower estuary.

The high organic matter inputs and their subsequent oxidation also appear essential for developing low-oxygen conditions in this region. When the vertical exchange of dissolved materials is limited by intensive stratification, the regeneration of nutrients below the pycnocline is mainly governed by organic matter remineralization (Zhu et al., 2011; Wang et al., 2016). The C/N ratio may thus be a useful first order indicator of the composition of the organic matter being respired. We adopted the following reaction, modified from Liu et al. (2015), illustrating the stoichiometric relationship between DO consumption and C/N ratios during aerobic respiration.



where, r is the C/N atomic ratio, and a , the coefficient of O_2 , depends on the end-products and their proportions.

The coefficient of O_2 (a) changes from $16r$ to $16(r+2)$ mol O_2 per mol organic matter when the oxidative products of nitrogen shift from 16NH_3 to 16HNO_3 . Therefore, the atomic ratio of DO consumed to all DIN products ranged between r (when DIN products were 16NH_3) and $r+2$ (when DIN products were 16HNO_3). We plotted the magnitude of DO depletion (i.e., the difference between the measured DO concentration and the equilibrium saturation concentration for a given water mass in $\mu\text{mol kg}^{-1}$) versus DIN concentrations for bottom layer waters of summer, resulting in a linear regression with a slope of ~ 7 ($r = 0.62$, $p < 0.001$, $n = 38$) (Fig. 7e). This slope implied that the organic matter decomposing under the pycnocline has a low C/N ratio ($\sim 5\text{--}7$), highly resembling marine organic matter ($\text{C/N} = 6.5 \pm 0.1$) rather than terrestrial

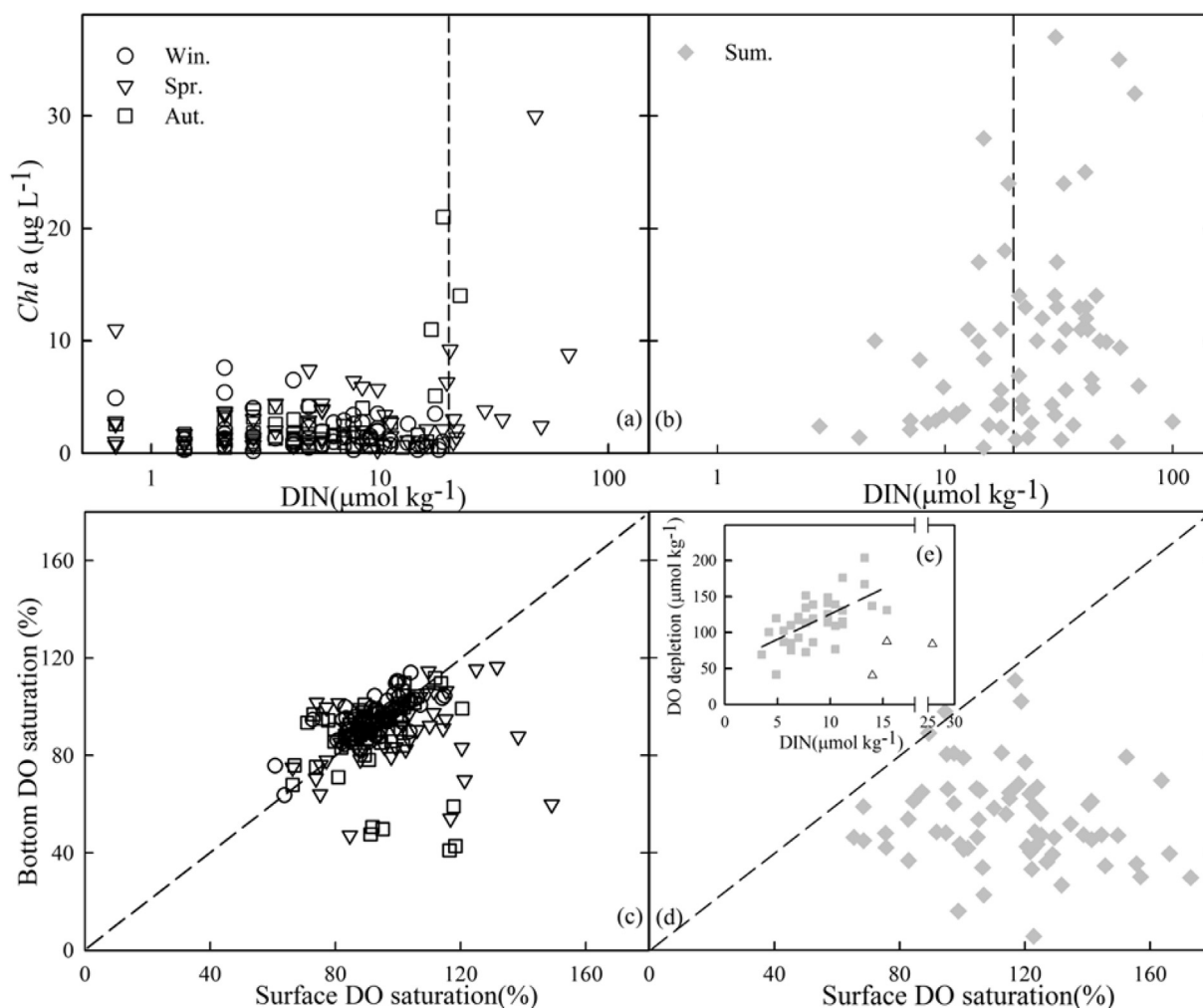


Fig. 7. (a), (b) *Chl a* versus DIN in surface layer. (c), (d) DO saturations (%) in surface and bottom layers as a function of season at Station SM18. Dashed lines denote 20 μmol kg⁻¹ for DIN and 1:1 ratio for DO saturation, respectively. (e) DO depletion versus DIN in the bottom layer of Station SM18 in July and August when DO depletion was frequently observed. The dashed line shows the linear regression (DO depletion = $(-7.0 \pm 1.5) \text{DIN} + (55.4 \pm 13.6)$, $r = 0.62$, $p < 0.01$, $n = 38$) based on all samples except for the three outliers denoted by triangles.

particulate matter ($C/N = 13.3 \pm 1.4$) in the PRE (Zhang et al., 2009; He et al., 2010; Yu et al., 2010). Along with the $\delta^{13}\text{C}$ signal of degraded organic carbon, which shows that marine sourced organic matter dominates DO consumption with a smaller contribution from terrestrially sourced organic matter (Hu et al., 2006; Su et al., 2017), the DIN/DO ratio presented here further reveals the stoichiometry of subsurface hypoxic water.

It was believed that hypoxia in the lower PRE is episodic because of its shallow depth and strong hydrodynamic changes driven by wind direction and strength (Yin et al., 2004b; Rabouille et al., 2008). Most of the Lingdingyang bay is quite shallow (~5 m), although the water depth is ~20 m off the Lingdingyang bay and in nearby regions, where hypoxia has been frequently reported in recent works (Su et al., 2017; Ye et al., 2013). Wind events can destratify the water column; however, vertical stratification and DO-depletion can quickly reinstate after the passage of a typhoon in the same area (Su et al., 2017). Thus, the proper water depth and water column stability, together with enhanced aerobic respiration, is conducive to a hypoxia-prone area in the lower PRE in summer.

Significant warming has been observed in the world's oceans resulting in a decrease in O₂ solubility (Keeling and Garcia, 2002). A warming rate of $-0.05 \text{ }^\circ\text{C yr}^{-1}$ was reported for coastal China Seas

(Lima and Wetthey, 2012). Considering brackish water as an example ($S = 30$, $T = 20 \text{ }^\circ\text{C}$), this rapid warming rate would yield a rate of decline of $0.2 \text{ } \mu\text{mol DO kg}^{-1} \text{ yr}^{-1}$ based on the solubility of oxygen. This result is consistent with the deoxygenation rate ($0.2\text{--}0.7 \text{ } \mu\text{mol kg}^{-1} \text{ yr}^{-1}$) in the subsurface layer on the outer shelf and in the open ocean (Whitney et al., 2007; Takatani et al., 2012), but merely accounts for ~10% of the DO decline revealed off Hong Kong.

We also note that upwelling provides relatively lower DO and nutrient-replete deep waters that could also stimulate hypoxia in some estuaries and/or coastal systems (Glenn et al., 2004; Grantham et al., 2004; Monteiro et al., 2006; Qian et al., 2017). The subsurface South China Sea water could indeed extend into the inner shelf and interact with the Pearl River plume (Gan et al., 2009; Cao et al., 2011; Han et al., 2012; Wu et al., 2017). However, the estimated deoxygenation rate in the bottom layer based on annual minimum DO saturation states cannot be explained by more intense upwelling during the last twenty years since we do not see a significant cooling trend in bottom waters (see in Fig. 6e). Moreover, the average temperature of bottom water was $\sim 24 \text{ }^\circ\text{C}$ in July and August, which can be traced to ~50 m depth directly below the seasonal mixing layer, where DO is still replete (Chen et al.,

2006; Wong et al., 2015). Thus, upwelling of low DO waters contributes little to the observed deoxygenation trend in the bottom layer under study.

In summary, the seasonality of local hydrology, DO variations, and the stoichiometric pattern between DO depletion and DIN, suggests a cascading linkage between the exacerbation of eutrophic conditions, enhanced local productivity, and the emergence of seasonal DO deficiency and/or hypoxia.

5. Concluding remarks

This study clearly shows seasonal DO deficiency and its evolution in the lower PRE based on a unique dataset including monthly cruises during 2010–2011 and long-term monitoring data off Hong Kong. The annual cycles observed in the measured parameters indicate that DO-deficient water most likely develops during summer in the lower estuary where physical and biological factors are conducive to its formation, very likely associated with excessive production during seasonal phytoplankton bloom stimulated by excessive nutrient runoff. Meanwhile, the rapid decline of annual minimum DO saturation states in bottom waters ($\sim 2 \pm 0.9 \mu\text{mol kg}^{-1} \text{yr}^{-1}$) over the last 25 years well illustrated the trend of seasonal deoxygenation in the lower estuary, which will likely develop into large areas of seasonal hypoxia as being seen in the East China Sea off the Changjiang estuary and in the Bohai Sea (Li et al., 2002; Zhai et al., 2012; Zhao et al., 2017).

Acknowledgements

This study was partially supported by a grant from the Research Grants Council of the Hong Kong Special Administrative Region, China (Project No. T21-602/16R), by the National Natural Science Foundation of China through Grants 41361164001, and by the Ocean Public Welfare Scientific Research Project, State Oceanic Administration of China through Grant 201505003-3. Wei Qian was partially supported by the Innovative Research Team Program of Fujian Normal University, China (IRTL1205). We thank greatly all participants of the monthly cruises during 2010–2011. Professor S-J Kao provided constructive comments on the earlier version of this work. Huade Zhao, Chuanjun Du, Yanping Xu and Jianzhong Su are appreciated for their help. We are also grateful to the Captain and crews of *Yue Dongguan 00589* for their assistance during the sampling cruises.

Appendix A. Supplementary data

Supplementary data related to this article can be found at <https://doi.org/10.1016/j.jecss.2018.03.004>.

References

- Alvisi, F., Cozzi, S., 2016. Seasonal dynamics and long-term trend of hypoxia in the coastal zone of Emilia Romagna (NW Adriatic Sea, Italy). *Sci. Total Environ.* 541, 1448–1462.
- Bianchi, T.S., Allison, M.A., 2009. Large-river delta-front estuaries as natural "recorders" of global environmental change. *Proc. Natl. Acad. Sci.* 106, 8085–8092.
- Cai, W.-J., Hu, X.P., Huang, W.-J., Murrell, M.C., Lehrter, J.C., Lohrenz, S.E., Chou, W.-C., Zhai, W.D., Hollibaugh, J.T., Wang, Y.C., Zhao, P.S., Guo, X.H., Gundersen, K., Dai, M.H., Gong, G.-C., 2011. Acidification of subsurface coastal waters enhanced by eutrophication. *Nat. Geosci.* 4 (11), 766–770.
- Cao, Z.M., Dai, M.H., Zheng, N., Wang, D.L., Li, Q., Zhai, W.D., Meng, F.F., Gan, J.P., 2011. Dynamics of the carbonate system in a large continental shelf system under the influence of both a river plume and coastal upwelling. *J. Geophys. Res.: Biogeosci.* 116 (G2), G02010.
- Chen, C.-C., Gong, G.-C., Shiah, F.-K., 2007. Hypoxia in the East China Sea: one of the largest coastal low-oxygen areas in the world. *Mar. Environ. Res.* 64 (4), 399–408.
- Chen, C.-T.A., Hou, W.-P., Gamo, T., Wang, S.L., 2006. Carbonate-related parameters of subsurface waters in the West Philippine, South China and Sulu Seas. *Mar. Chem.* 99 (1), 151–161.
- Dai, M.H., Gan, J.P., Han, A.Q., Kung, H.S., Yin, Z.Q., 2014. Physical dynamics and biogeochemistry of the Pearl river plume. In: Bianchi, T.S., Allison, M.A., Cai, W.J. (Eds.), *Biogeochemical Dynamics at Major River-Coastal Interfaces Linkages with Global Change*. Cambridge University Press, pp. 321–352.
- Dai, M.H., Guo, X.H., Zhai, W.D., Yuan, L.Y., Wang, B.W., Wang, L.F., Cai, P.H., Tang, T.T., Cai, W.-J., 2006. Oxygen depletion in the upper reach of the Pearl river estuary during a winter drought. *Mar. Chem.* 102 (1), 159–169.
- Dai, M.H., Wang, L.F., Guo, X.H., Zhai, W.D., Li, Q., He, B.Y., Kao, S.-J., 2008. Nitrification and inorganic nitrogen distribution in a large perturbed river/estuarine system: the Pearl river Estuary, China. *Biogeosci. Discuss.* 5 (2), 1545–1585.
- Diaz, R.J., Rosenberg, R., 2008. Spreading dead zones and consequences for marine ecosystems. *Science* 321 (5891), 926–929 doi:10.1126/science.1156401.
- Friedrich, J., Janssen, F., Aleynik, D., Bange, H.W., Boltacheva, N., Gagatay, M.N., Dale, A.W., Etiope, G., Erdem, Z., Geraga, M., Gilli, A., Gomoiu, M.T., Hall, P.O.J., Hansson, D., He, Y., Holtappels, M., Kirf, M.K., Kononets, M., Kononov, S., Lichtschlag, A., Livingstone, D.M., Marinaro, G., Mazlumyan, S., Naeher, S., North, R.P., Papatheodorou, G., Pfannkuche, O., Prien, R., Rehder, G., Schubert, C.J., Soltwedel, T., Sommer, S., Stahl, H., Stanev, E.V., Teaca, A., Tengberg, A., Waldmann, C., Wehrli, B., Wenzhöfer, F., 2014. Investigating hypoxia in aquatic environments: diverse approaches to addressing a complex phenomenon. *Biogeosciences* 11 (4), 1215–1259.
- Gan, J.P., Li, L., Wang, D.X., Guo, X.G., 2009. Interaction of a river plume with coastal upwelling in the northeastern South China Sea. *Continent. Shelf Res.* 29 (4), 728–740.
- Glenn, S., Arnone, R., Bergmann, T., Bissett, W.P., Crowley, M., Cullen, J., Gryzmski, J., Haidvogel, D., Kohut, J., Moline, M., Oliver, M., Orrico, C., Sherrell, R., Song, T., Weidemann, A., Chant, R., Schofield, O., 2004. Biogeochemical impact of summertime coastal upwelling on the New Jersey Shelf. *J. Geophys. Res.: Oceans* 109 (C12), C12S02.
- Grantham, B.A., Chan, F., Nielsen, K.J., Fox, D.S., Barth, J.A., Huyer, A., Lubchenco, J., Menge, B.A., 2004. Upwelling-driven nearshore hypoxia signals ecosystem and oceanographic changes in the northeast Pacific. *Nature* 429 (6993), 749–754 doi:10.1038/nature02605.
- Guo, X.H., Dai, M.H., Zhai, W.D., Cai, W.-J., Chen, B.S., 2009. CO₂ flux and seasonal variability in a large subtropical estuarine system, the Pearl river Estuary, China. *J. Geophys. Res.: Biogeosciences* 114 (G3), G03013.
- Han, A.Q., Dai, M.H., Kao, S.-J., Gan, J.P., Li, Q., Wang, L.F., Zhai, W.D., Wang, L., 2012. Nutrient dynamics and biological consumption in a large continental shelf system under the influence of both a river plume and coastal upwelling. *Limnol. Oceanogr.* 57 (2), 486–502.
- Harrison, P.J., Yin, K.D., Lee, J.H.W., Gan, J.P., Liu, H.B., 2008. Physical–biological coupling in the Pearl river estuary. *Continent. Shelf Res.* 28 (12), 1405–1415.
- He, B.Y., Dai, M.H., Huang, W., Liu, Q., Chen, H.M., Xu, L., 2010. Sources and accumulation of organic carbon in the Pearl River Estuary surface sediment as indicated by elemental, stable carbon isotopic, and carbohydrate compositions. *Biogeosciences* 7 (10), 3343–3362.
- He, B.Y., Dai, M.H., Zhai, W.D., Guo, X.H., Wang, L.F., 2014. Hypoxia in the upper reaches of the Pearl River Estuary and its maintenance mechanisms: a synthesis based on multiple year observations during 2000–2008. *Mar. Chem.* 167, 13–24.
- Herbland, A., Le Bouteiller, A., Raimbault, P., 1985. Size structure of phytoplankton biomass in the equatorial Atlantic Ocean. *Deep-Sea Res. Part A Oceanogr. Res. Pap.* 32 (7), 819–836.
- Hu, J.F., Peng, P.A., Jia, G.D., Mai, B.X., Zhang, G., 2006. Distribution and sources of organic carbon, nitrogen and their isotopes in sediments of the subtropical Pearl River Estuary and adjacent shelf, Southern China. *Mar. Chem.* 98 (2–4), 274–285.
- Jia, G.D., Peng, P.A., 2003. Temporal and spatial variations in signatures of sedimented organic matter in Lingding Bay (Pearl estuary), Southern China. *Mar. Chem.* 82 (1–2), 47–54.
- Keeling, R.F., Garcia, H.E., 2002. The change in oceanic O₂ inventory associated with recent global warming. *Proc. Natl. Acad. Sci.* 99 (12), 7848–7853 doi:10.1073/pnas.122154899.
- Kristiansen, K.D., Kristensen, E., Jensen, E.M.H., 2002. The influence of water column hypoxia on the behaviour of manganese and iron in sandy coastal marine sediment. *Estuar. Coast Shelf Sci.* 55 (4), 645–654.
- Levin, L.A., Ekau, W., Gooday, A.J., Jorissen, F., Middelburg, J.J., Naqvi, S.W.A., Neira, C., Rabalais, N.N., Zhang, J., 2009. Effects of natural and human-induced hypoxia on coastal benthos. *Biogeosciences* 6 (10), 2063–2098.
- Li, D.J., Zhang, J., Huang, D.J., Wu, Y., Liang, J., 2002. Oxygen depletion off the Changjiang (Yangtze River) estuary. *Sci. China Earth Sci.* 45 (12), 1137–1146.
- Lima, F.P., Wetzel, D.S., 2012. Three decades of high-resolution coastal sea surface temperatures reveal more than warming. *Nat. Commun.* 3, 704.
- Lin, H., Dai, M., Kao, S.-J., Wang, L., Roberts, E., Yang, J.-Y.T., Huang, T., He, B., 2016. Spatiotemporal variability of nitrous oxide in a large eutrophic estuarine system: the Pearl River Estuary, China. *Mar. Chem.* 182, 14–24.
- Lin, H.Y., Liu, S., Han, W.Y., 2001. Potential trigger CTB, from seasonal bottom hypoxia in the Pearl River Estuary. *J. Zhanjiang Ocean Univ.* 21, 25–29 in Chinese with English abstract.
- Liu, K.-K., Yan, W.J., Lee, H.-J., Chao, S.-Y., Gong, G.-C., Yeh, T.-Y., 2015. Impacts of increasing dissolved inorganic nitrogen discharged from Changjiang on primary production and seafloor oxygen demand in the East China Sea from 1970 to 2002. *J. Mar. Syst.* 141, 200–217.
- Lu, F.H., Ni, H.G., Liu, F., Zeng, E.Y., 2009. Occurrence of nutrients in riverine runoff of

- the Pearl River Delta, South China. *J. Hydrol.* 376 (1), 107–115.
- Lu, Z.M., Gan, J.P., 2015. Controls of seasonal variability of phytoplankton blooms in the Pearl River Estuary. *Deep Sea Res. Part II Top. Stud. Oceanogr.* 117, 86–96.
- Lui, H.-K., Chen, C.-T.A., 2011. Shifts in limiting nutrients in an estuary caused by mixing and biological activity. *Limnol. Oceanogr.* 56 (3), 989–998.
- Lui, H.-K., Chen, C.-T.A., 2012. The nonlinear relationship between nutrient ratios and salinity in estuarine ecosystems: implications for management. *Curr. Opin. Environ. Sustain.* 4 (2), 227–232.
- Luo, L., Li, S.Y., Li, H.M., 2005. Characteristics of dissolved oxygen and its affecting factors in the Pearl River Estuary in summer. *Acta Sci. Nat. Univ. Sunyatseni* 44 (6), 118–122 in Chinese with English abstract.
- Middelburg, J., Levin, L., 2009. Coastal hypoxia and sediment biogeochemistry. *Biogeosciences* 6 (7), 1273–1293.
- Monteiro, P.M.S., van der Plas, A., Mohrholz, V., Mabilhe, E., Pascall, A., Joubert, W., 2006. Variability of natural hypoxia and methane in a coastal upwelling system: oceanic physics or shelf biology? *Geophys. Res. Lett.* 33 (16), L16614.
- Ou, S.Y., Zhang, H., Wang, D.X., 2009. Dynamics of the buoyant plume off the Pearl River estuary in summer. *Environ. Fluid Mech.* 9 (5), 471–492.
- Parsons, T.R., Maita, Y., Lalli, C.M., 1984. *A Manual of Chemical and Biological Method for Seawater Analysis*. Pergamon Press, Oxford, pp. 101–103.
- Qian, W., Dai, M.H., Xu, M., Kao, S.-J., Du, C.J., Liu, J.W., Wang, H.J., Guo, L.G., Wang, L.F., 2017. Non-local drivers of the summer hypoxia in the East China Sea off the Changjiang estuary. *Estuar. Coast Shelf Sci.* 198 (Part B), 393–399.
- Qu, T.D., Kim, Y.Y., Yaremchuk, M., Tozuka, T., Ishida, A., Yamagata, T., 2004. Can luzon strait transport play a role in conveying the impact of ENSO to the South China Sea? *J. Clim.* 17 (18), 3644–3657.
- Rabalais, N.N., Turner, R.E., Wiseman, W.J., 2002. Gulf of Mexico hypoxia, A.K.A. “the dead zone”. *Annu. Rev. Ecol. Systemat.* 33 (1), 235–263.
- Rabouille, C., Conley, D.J., Dai, M.H., Cai, W.J., Chen, C.T.A., Lansard, B., Green, R., Yin, K., Harrison, P.J., Dagg, M., McKee, B., 2008. Comparison of hypoxia among four river-dominated ocean margins: the Changjiang (Yangtze), Mississippi, Pearl, and Rhône rivers. *Continental Shelf Res.* 28 (12), 1527–1537.
- Shen, J., Wang, T.P., Herman, J., Mason, P., Arnold, G.L., 2008. Hypoxia in a coastal embayment of the Chesapeake Bay: a model diagnostic study of oxygen dynamics. *Estuar. Coast* 31 (4), 652–663.
- Su, J.L., 2004. Overview of the South China Sea circulation and its influence on the coastal physical oceanography outside the Pearl River estuary. *Continental Shelf Res.* 24 (16), 1745–1760.
- Su, J.Z., Dai, M.H., He, B.Y., Wang, L.F., Gan, J.P., Guo, X.H., Zhao, H.D., Yu, F.L., 2017. Tracing the origin of the oxygen-consuming organic matter in the hypoxic zone in a large eutrophic estuary: the lower reach of the Pearl River Estuary, China. *Biogeosciences* 14, 4085–4099.
- Takatani, Y., Sasano, D., Nakano, T., Midorikawa, T., Ishii, M., 2012. Decrease of dissolved oxygen after the mid-1980s in the western North Pacific subtropical gyre along the 137°E repeat section. *Global Biogeochem. Cycles* 26 (2), GB2013.
- Tang, D.L., Kester, D.R., Ni, I.H., Qi, Y.Z., Kawamura, H., 2003. In situ and satellite observations of a harmful algal bloom and water condition at the Pearl River Estuary in late autumn 1998. *Harmful Algae* 2 (2), 89–99.
- Wang, D.L., Lin, W.F., Yang, X.Q., Zhai, W.D., Dai, M.H., Arthur Chen, C.-T., 2012. Occurrences of dissolved trace metals (Cu, Cd, and Mn) in the Pearl River Estuary (China), a large river-groundwater-estuary system. *Continental Shelf Res.* 50–51, 54–63.
- Wang, H.J., Dai, M.H., Liu, J.W., Kao, S.-J., Zhang, C., Cai, W.-J., Wang, G.Z., Qian, W., Zhao, M.X., Sun, Z.Y., 2016. Eutrophication-driven hypoxia in the east China Sea off the Changjiang estuary. *Environ. Sci. Technol.* 50 (5), 2255–2263.
- Wang, Z.-H., Feng, J., Nie, X.-P., 2015. Recent environmental changes reflected by metals and biogenic elements in sediments from the Guishan Island, the Pearl River Estuary, China. *Estuar. Coast Shelf Sci.* 164, 493–505.
- Whitney, F.A., Freeland, H.J., Robert, M., 2007. Persistently declining oxygen levels in the interior waters of the eastern subarctic Pacific. *Prog. Oceanogr.* 75 (2), 179–199.
- Wong, G.T.F., Pan, X.J., Li, K.-Y., Shiah, F.-K., Ho, T.-Y., Guo, X.H., 2015. Hydrography and nutrient dynamics in the northern South China sea Shelf-sea (NoSoCS). *Deep Sea Res. Part II Top. Stud. Oceanogr.* 117, 23–40.
- Wu, C.S., Yang, S.L., Huang, S.C., Mu, J.B., 2016. Delta changes in the Pearl River Estuary and its response to human activities (1954–2008). *Quat. Int.* 392, 147–154.
- Wu, K., Dai, M.H., Li, X.L., Meng, F.F., Chen, J.H., Lin, J.R., 2017. Dynamics and production of dissolved organic carbon in a large continental shelf system under the influence of both river plume and coastal upwelling. *Limnol. Oceanogr.* 62 (3), 973–988.
- Xu, J., Ho, A.Y.T., Yin, K.D., Yuan, X.C., Anderson, D.M., Lee, J.H.W., Harrison, P.J., 2008. Temporal and spatial variations in nutrient stoichiometry and regulation of phytoplankton biomass in Hong Kong waters: influence of the Pearl River outflow and sewage inputs. *Mar. Pollut. Bull.* 57 (6–12), 335–348.
- Xu, J., Lee, J.H.W., Yin, K.D., Liu, H.B., Ho, A.Y.T., Yuan, X.C., Harrison, P.J., 2011. Environmental response to sewage treatment strategies: Hong Kong’s experience in long term water quality monitoring. *Mar. Pollut. Bull.* 62 (11), 2275–2287.
- Xu, J., Yin, K.D., Lee, J.H.W., Liu, H.B., Ho, A.Y.T., Yuan, X.C., Harrison, P.J., 2010. Long-term and seasonal changes in nutrients, phytoplankton biomass, and dissolved oxygen in deep bay, Hong Kong. *Estuar. Coast* 33 (2), 399–416.
- Yan, X.L., Zhai, W.D., Hong, H.S., Li, Y., Guo, W.D., Huang, X., 2012. Distribution, fluxes and decadal changes of nutrients in the Jiulong River Estuary, southwest Taiwan strait. *Chin. Sci. Bull.* 57 (18), 2307–2318.
- Ye, F., Huang, X.P., Shi, Z., Liu, Q.X., 2013. Distribution characteristics of dissolved oxygen and its affecting factors in the Pearl River Estuary during the summer of the extremely drought hydrological year 2011. *Environ. Sci. (in Chinese)* 34 (5), 1707–1714.
- Ye, F., Huang, X.P., Zhang, X., Zhang, D.W., Zeng, Y.Y., Tian, L., 2012. Recent oxygen depletion in the Pearl River Estuary, South China: geochemical and microfaunal evidence. *J. Oceanogr.* 68 (3), 387–400.
- Yin, K.D., Lin, Z.F., Ke, Z.Y., 2004a. Temporal and spatial distribution of dissolved oxygen in the Pearl River Estuary and adjacent coastal waters. *Continental Shelf Res.* 24 (16), 1935–1948.
- Yin, K.D., Zhang, J.L., Qian, P.-Y., Jian, W.J., Huang, L.M., Chen, J.F., Wu, M.C.S., 2004b. Effect of wind events on phytoplankton blooms in the Pearl River Estuary during summer. *Continental Shelf Res.* 24 (16), 1909–1923.
- Yu, F.L., Zong, Y.Q., Lloyd, J.M., Huang, G.Q., Leng, M.J., Kendrick, C., Lamb, A.L., Yim, W.W.S., 2010. Bulk organic $\delta^{13}\text{C}$ and C/N as indicators for sediment sources in the Pearl River delta and estuary, Southern China. *Estuar. Coast Shelf Sci.* 87 (4), 618–630.
- Zhai, W.D., Dai, M.H., Cai, W.-J., Wang, Y.C., Wang, Z.H., 2005. High partial pressure of CO_2 and its maintaining mechanism in a subtropical estuary: the Pearl River Estuary, China. *Mar. Chem.* 93 (1), 21–32.
- Zhai, W.D., Zhao, H.D., Zheng, N., Xu, Y., 2012. Coastal acidification in summer bottom oxygen-depleted waters in northwestern-northern Bohai Sea from June to August in 2011. *Chin. Sci. Bull.* 57 (9), 1062–1068.
- Zhang, J., Gilbert, O., Gooday, A.J., Levin, L., Naqvi, S.W.A., Middelburg, J.J., Scranton, M., Ekau, W., Peña, A., Dewitte, B., Oguz, T., Monteiro, P.M.S., Urban, E., Rabalais, N.N., Ittekkot, V., Kemp, W.M., Ulloa, O., Elmgren, R., Escobar-Brienes, E., Van der Plas, A.K., 2010. Natural and human-induced hypoxia and consequences for coastal areas: synthesis and future development. *Biogeosciences* 7 (5), 1443–1467.
- Zhang, L., Yin, K.D., Wang, L., Chen, F.R., Zhang, D.R., Yang, Y.Q., 2009. The sources and accumulation rate of sedimentary organic matter in the Pearl River Estuary and adjacent coastal area, Southern China. *Estuar. Coast Shelf Sci.* 85 (2), 190–196.
- Zhao, H.D., Kao, S.-J., Zhai, W.D., Zang, K.P., Zheng, N., Xu, X.M., Huo, C., Wang, J.Y., 2017. Effects of stratification, organic matter remineralization and bathymetry on summertime oxygen distribution in the Bohai Sea, China. *Continental Shelf Res.* 134, 15–25.
- Zhu, J.R., Zhu, Z.Y., Lin, J., Wu, H., Zhang, J., 2016. Distribution of hypoxia and pycnocline off the Changjiang Estuary, China. *J. Mar. Syst.* 154 (Part A), 28–40.
- Zhu, Z.Y., Zhang, J., Wu, Y., Zhang, Y.Y., Lin, J., Liu, S.M., 2011. Hypoxia off the Changjiang (yangtze River) estuary: oxygen depletion and organic matter decomposition. *Mar. Chem.* 125 (1–4), 108–116.
- Zu, T.T., Gan, J.P., 2015. A numerical study of coupled estuary–shelf circulation around the Pearl River Estuary during summer: responses to variable winds, tides and river discharge. *Deep Sea Res. Part II Top. Stud. Oceanogr.* 117, 53–64.
- Zu, T.T., Wang, D.X., Gan, J.P., Guan, W.B., 2014. On the role of wind and tide in generating variability of Pearl River plume during summer in a coupled wide estuary and shelf system. *J. Mar. Syst.* 136, 65–79.